Received: 19 January 2022 | Revised: 9 May 2022 | Accepted: 9 May 2022

DOI: 10.1002/app.52823

RESEARCH ARTICLE

Applied Polymer SCIENCE WILEY

Fabrication and evaporation time investigation of water treatment membranes using green solvents and recycled polyethylene terephthalate

David Lu[1] | Parto Babaniamansour[2] | Alex Williams[1] | Kassandra Opfar[1] | Parker Nurick[1] | Isabel C. Escobar[1]

[1]Department of Chemical and Materials Engineering, University of Kentucky, Lexington, Kentucky, USA

[2]F. Joseph Halcomb III, M.D. Department of Biomedical Engineering, University of Kentucky, Lexington, Kentucky, USA

Correspondence
Isabel C. Escobar, Department of Chemical and Materials Engineering, University of Kentucky, 177 F. Paul Anderson Tower, Lexington, KY 40506-0046, USA.
Email: isabel.escobar@uky.edu

Funding information
National Science Foundation, Grant/Award Numbers: 2121674, 1922694

Abstract

Many materials traditionally used for polymeric membrane fabrication incur significant environmental impacts and limit sustainability of the process; therefore, more eco-friendly materials are needed in membrane fabrication. In this study, recycled polyethylene terephthalate (rPET) and a solvent blend of Rhodiasolv® PolarClean (PolarClean) and gamma-valerolactone (GVL) were used as eco-friendly materials to fabricate polysulfone (PSf) ultrafiltration membranes. The calculated Hansen solubility parameter affinity and relative energy difference values for PET and PolarClean-GVL of 6.94 and 0.86, respectively, indicate favorable dissolution to create the preceding dope solution. At a baseline evaporation time of 30 s, the resulting rPET-PSf/PolarClean-GVL membranes outperformed the filtration capabilities of PSf/NMP membranes with 3.5% higher permeability (23.4 LMH/bar) and 53.2% greater rejection (84.9%) of bovine serum albumin (BSA). Increasing the evaporation time to 60 s resulted in a 32.4 LMH/bar decrease in permeability and 0.8% increase in BSA rejection, whereas decreasing the evaporation time to 0 s generally led to a 235.8 LMH/bar increase in permeability and 4% increase in BSA rejection. The findings indicate the potential for eco-friendly materials to serve as alternatives for traditional materials in polymeric membranes.

KEYWORDS

blends, membranes, recycling, synthesis and processing techniques

1 | INTRODUCTION

Membrane technology plays a critical role in water treatment and the importance of membranes has become more evident.[1] Polymeric membranes have become more prevalent in separation applications due to their desirable physical and chemical properties, including a variety of pore ranges and application modes.[2,3] Along with cost effectiveness, polymeric membranes are advantageous due to the relative ease in production, particularly via phase inversion methods.[4,5] While other innovative membrane fabrications have been developed,[6,7] phase inversion is currently the most widespread technique for polymeric membrane fabrication, in which the initial polymer solution begins to separate into a polymer-rich phase and polymer-poor phase that becomes thermodynamically instable.[8,9] The polymer lean-phase induces the porosity in the solidified material, while the polymer-rich phase forms a solid membrane matrix.[10]

Nonsolvent-induced phase separation (NIPS) is considered the dominant phase inversion method for fabricating a polymeric membrane with a dense surface and

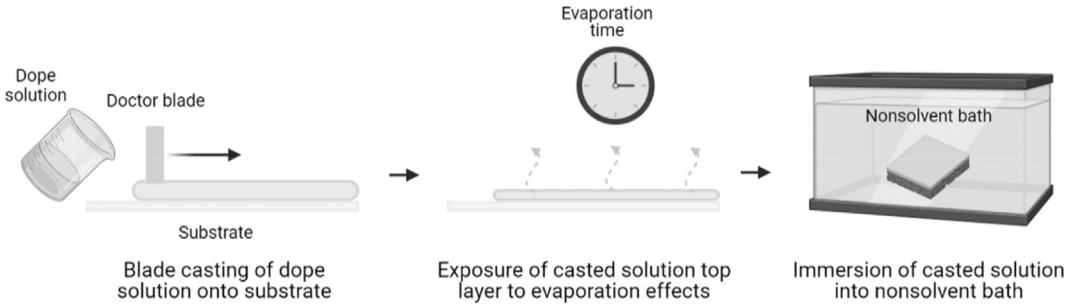

FIGURE 1 Overview of nonsolvent phase induced separation for polymeric membrane fabrication.

asymmetric pores.[11] As shown in Figure 1, the process begins with the formation of a homogenous dope solution consisting of a polymer or polymer mixture dissolved in at least one solvent; the solution may also contain pore formers or other additives that influence the membrane formation. Once uniform, the solution is casted as a liquid film on a solid substrate (commonly a glass plate or polymer substrate). The film and substrate are then immersed in a non-solvent bath (typically water), which induces phase separation, as the solvent in the film exchanges with the non-solvent.[12] The result of the mixing and de-mixing of the components is the formation of an asymmetric polymeric membrane with a dense selective layer and a porous support layer underneath it; the top layer provides separation selectivity due to size exclusion or charge, whereas the bottom layer provides mechanical support and stability.[12]

The final membrane structure and performance characteristics depend on many phase inversion parameters, such as the type of polymer and solvent, polymer concentration, dope solution evaporation time, and the casting technique.[13] In particular, evaporation time is the amount of time the solution film is exposed to air before immersion in the nonsolvent bath.[10] This process causes partial evaporation of solvent from the top layer and increases the local polymer concentration; the altered top layer acts as a resistance barrier between the nonsolvent bath and bulk membrane layers, thus limiting diffusion of nonsolvent into the membrane.[10] Understanding the relationship between evaporation time and the final membrane structure and filtration properties can lead to determining an evaporation time duration that optimizes these characteristics.

One current drawback to most polymeric membranes is the use of hazardous and petroleum-based polymer and solvent materials. Traditional solvents, including NMP, dimethylacetamide (DMAc), and dimethylformamide (DMF), are considered hazardous to human health and the environment due to high levels of toxicity, irritability, flammability, and carcinogenicity.[5,14–16] During phase inversion, solvent from the dope solution leaches into the nonsolvent bath due to solvent-nonsolvent diffusion.[5,17] Improper treatment and disposal of industrial membrane fabrication wastewater is an imperative concern; a survey conducted by Razali et al.[17] reported that the majority of 13 commercial membrane manufacturing companies did not adequately treat membrane fabrication wastewater. Furthermore, an estimated annual amount of over 100 billion liters of wastewater is generated and released from the industrial membrane manufacturing sector, which compounds the hazards.[17]

Similarly, many polymers commonly used in polymeric membranes are considered unsustainable since they are derived from petrochemicals. Traditional synthetic polymers, including PSf, poly (vinylidene fluoride) (PVDF), and polyethersulfone (PES), are ideal for phase inversion fabrication and water treatment applications due to low manufacturing costs and strong chemical and thermal stability.[18–20] However, new environmental regulations have also increased the demand for polymers that can be sustainably produced and disposed with a smaller environmental impact, including a recent ban on NMP by the European Union.[5,21] Therefore, the use of more eco-friendly polymers and solvents (i.e., possessing non-toxic, bio-derived, and/or biodegradable qualities) in membranes has become a growing field of research.[22] Along with these eco-friendly qualities, membranes fabricated from such components should parallel the performance characteristics of traditional solvent-based polymeric membranes.

Two bio-derived solvents of interest are methyl 5-(dimethylamino)-2-methyl-5-oxopentanoate (Rhodiasolv® PolarClean) and gamma-valerolactone (GVL). PolarClean is derived from a by-product of Nylon 6,6 fabrication and is commercialized by Solvay Novecare.[12,23,24] GVL is produced from the processing of hemicellulose and cellulose; both biomaterials undergo acid hydrolysis to form ethyl levulinate and levulinic acid that are then hydrogenated to form GVL.[12,25]

As for eco-friendly polymers, recycled polyethylene terephthalate (rPET) is a promising candidate; PET is

commonly used for manufacturing bottles due to the inherent properties it provides, including optical transparency, moderate water vapor transmission rates, and low carbon dioxide transmission rates.[26] As such, PET accounts for a significant amount of plastic production, totaling to 18.8 million tons out of 269 million tons of plastic produced in 2015.[27] However, PET is difficult to naturally degrade, which can lead to substantial environmental plastic pollution.[27] Using a recyclable polymer and bio-derived solvents could increase the sustainability of polymeric membranes by reducing fossil fuel dependence and creating a high-value niche for plastic product recycling that could reduce pollution.[28]

Although the field of green material-based membranes is still emerging, several studies have investigated the use of rPET, PolarClean, and GVL as alternative membrane materials. Doan et al.[29] fabricated PDMS-functionalized rPET membranes capable of oil–water separation at a maximum flux of approximately 20,000 LMH and separation efficiency greater than 98%. Arahman et al.[30] reported the fabrication of PET membranes derived from plastic bottle waste that filtered humic acid from water at a maximum flux of 72.0 LMH and rejection of 75.92.[30] Several studies have incorporated PolarClean as a membrane solvent using other phase inversion methods, though its use via NIPS has not been extensively studied.[23,31,32] Dong et al.[33] reported the fabrication of PSf UF membranes using PolarClean and GVL as a solvent mixture via NIPS. Membranes fabricated solely with PolarClean exhibited collapsed pores during filtration, whereas membranes made with only GVL hydrolyzed.[33] When the solvents were combined, the resulting membranes filtered an aqueous bovine serum albumin (BSA) solution at a flux of 115 LMH and a BSA rejection of 99.2% ± 0.1%, which were similar to the performance parameters of a PSf membrane with DMAc as the solvent.[33] However, most studies have investigated membrane fabrication with a focus on a singular eco-friendly material; the use of rPET in tandem with bio-derived solvents for creating more eco-friendly polymeric membranes has not been reported in previous studies. Thus, this would be the first study to evaluate capitalizing on the benefits of both rPET and PolarClean-GVL in a polymeric membrane. Moreover, the role of evaporation time in influencing membrane performance has not been extensively studied either; an investigation into this fabrication parameter could provide more insight into optimizing eco-friendly material-based membrane performance.

In this study, lab-scale UF PSf membranes were fabricated via NIPS with the incorporation of PET (pristine and recycled), PolarClean, and GVL as eco-friendly materials. PSf was chosen as a polymer since it commonly used for commercial membranes and has not been extensively studied with eco-friendly materials before.[33] The thermodynamic aspects of a system comprised of these materials were assessed to determine the feasibility of forming a homogenous dope solution. The morphology and performance characteristics of the resulting membranes were compared to the characteristics of a traditional PSf-NMP membrane. Finally, the role of evaporation time on the membrane properties was investigated to determine an optimal specification for membrane performance.

2 | EXPERIMENT METHODOLOGY

2.1 | Materials

For this study, PSf was purchased from Sigma-Aldrich (St. Louis, MO) and PET pellets were purchased from Sigma-Aldrich. Recycled PET was sourced from a plastic water bottle. NMP was purchased from VWR; PolarClean was kindly provided by Solvay Novecare; GVL was purchased from Sigma-Aldrich. Phenol, ACS, 99+% was purchased from Sigma-Aldrich. Bovine serum albumin (BSA) was supplied from VWR Life Science. Galwick was purchased from Porous Materials Incorporated; isopropyl alcohol (IPA) was purchased from VWR. Grade I deionized (DI) water with resistivity of 18.2 mΩ cm at 25°C was provided by the Chemical Engineering Undergraduate Laboratory at the University of Kentucky.

2.2 | Thermodynamic study

2.2.1 | Hansen solubility study

Since the PET-PSf/PolarClean-GVL/water system is a novel solution for membrane fabrication, thermodynamic calculations were completed to determine the favorability of forming a homogenous dope solution. The experimental method for determining the solubility parameter of polymers commonly involves observing the swelling of the polymer as solvent is added. A solvent that leads to a greater degree of polymer swelling is considered an ideal solvent for that polymer. From Equation 1, a chemical reaction is thermodynamically favorable if:

$$\Delta G = \Delta H - T\Delta S < 0, \quad (1)$$

where ΔG is the change in Gibbs free energy, ΔH is the change in enthalpy, T is the temperature, and ΔS is the change in entropy. The mixture has more microstates than two separate components; therefore, entropy change is always positive. To induce one component to dissolve in another component, the enthalpy change should not

be highly positive. For predicting the solubility of two components, theoretical models, including the lattice model and the Flory-Huggins model, have been proposed to determine the magnitude of enthalpy and entropy. The later Hildebrand solubility model is a simple model for predicting nonpolar and slightly polar systems. In the Equation 2, E is cohesive energy, which is the amount of energy required to break the molecule into the gas. H_v is latent heat of vaporization, R is gas constant and T is the absolute temperature.

$$E = H_v - RT. \tag{2}$$

Since larger molecules have greater cohesive energy, the cohesive energy density (δ^2) is calculated by dividing it by molar volume V, as shown in Equation 3:

$$\delta^2 = \frac{\Delta H - RT}{V}. \tag{3}$$

A polymer is considered favorable for dissolution in a solvent when the solubility parameter is similar in value. Given that the Hildebrand solubility equation does not assume hydrogen bonding, the Hansen Solubility Model has been used for predicting solubility in this study since it accounts for this interaction.[34] Studying the solubility of polymer in solvent using the Hansen Solubility Model relies on the dispersion force (δ_d), polar force (δ_p), and hydrogen-binding (δ_h), as shown in Equation 4:

$$\delta^2 = {\delta_p}^2 + {\delta_d}^2 + {\delta_h}^2. \tag{4}$$

The three interaction parameters are factored into determining the affinity of the polymer and solvent (R_a), according to Equation 5:

$${R_a}^2 = 4(\delta_{d1} - \delta_{d2})^2 + (\delta_{p1} - \delta_{p2})^2 + (\delta_{h1} - \delta_{h2})^2. \tag{5}$$

Solubility increases as R_a approaches 0 since it indicates a close solubility parameter distance between the polymer and solvent.[33,34] According to the Hansen Solubility Model, the three interaction parameters form a sphere. The relative energy difference (RED), which describes the polymer-solvent interaction, can be determined from R_a, as shown in Equation 6:

$$\mathrm{RED} = \frac{R_a}{R_o}, \tag{6}$$

where R_o is the interaction radius of the Hansen solubility parameter sphere of the polymer; an RED value less than or equal to 1 indicates a favorable solvent for a polymer and, thus, favorability for the formation of a homogenous dope solution.[33]

TABLE 1 Dope solution polymer and solvent compositions for each membrane.

Membrane	Polymer composition	Solvent composition
M1	17 wt% PSf	83 wt% NMP
M2	17 wt% PSf	62.25 wt% PolarClean 20.75 wt% GVL
M3	2 wt% Pristine PET-dissolution agent 23 wt% PSf	56.25 wt% PolarClean 18.75 wt% GVL
M4	2 wt% Recycled PET-dissolution agent 23 wt% PSf	56.26 wt% PolarClean 18.75 wt% GVL

2.3 | Dope solution study

2.3.1 | Dope solution preparation

A comparative study between four types of polymeric membranes was conducted, as summarized in Table 1. The dope solution of M1, a membrane fabricated using a traditional solvent for use as a control, was fabricated by dissolving 17% PSf in NMP at room temperature for 72 h. For M2, NMP was substituted with a solvent mixture of PolarClean and GVL at a volumetric ratio of 3:1, which was found to produce membranes with an optimal balance of permeability and rejection capabilities.[35] PSf was mixed with the cosolvents at 80°C for 72 h. For M3, preparing a dope solution with PET and PSf as polymers with the PolarClean-GVL cosolvent mixture was a two-step process. First, 2% dissolved pristine PET was added to phenol and stirred at 80°C until the PET fully dissolved. The PolarClean-GVL mixture and PSf were then added to the solution and mixed at 80°C for 72 h. For M4, the plastic bottle was shredded into small pieces and substituted the pristine PET in the dope solution. Preparation of the dope solutions and fabrication of the resulting membranes is illustrated in Figure 2.

2.3.2 | PET solubility study

Due to the strong chemical resistance properties of PET, strong solvents are commonly used for dissolution. It was found that neither pristine PET nor rPET was fully

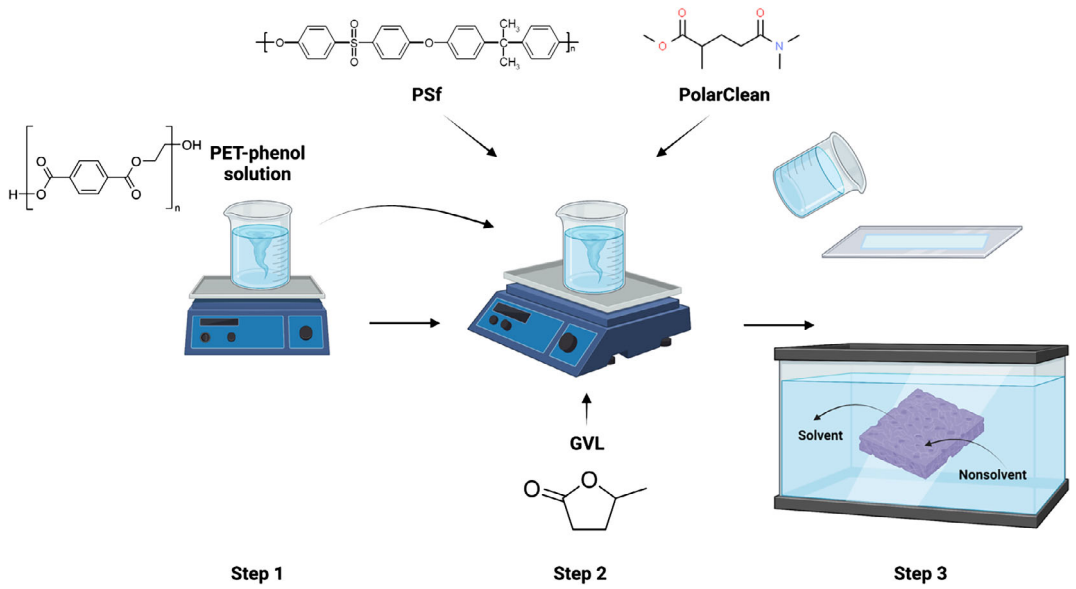

FIGURE 2 The schematic of the nonsolvent phase induced separation method used for fabrication of membrane with ultrafiltration and polyethylene terephthalate (PET) as polymers and PolarClean and gamma-valerolactone (GVL) as solvents. [Color figure can be viewed at wileyonlinelibrary.com]

soluble in the PolarClean-GVL mixture. Therefore, an intermediate dissolution agent was required for PET dissolution and a solubility study was performed using various common solvents and solvents used in similar studies.[29,36,37]

2.3.3 | Dope solution viscosity

Once the dope solutions were completely homogenized, the viscosity was measured using a Rheometer (AG-G2,TA instrument, DE) to determine the stress–strain behavior since dope solution viscosity can indicate the extent of homogeneity, as well as the membrane formation and performance profile. The solutions were subjected to a stress range of approximately 0–1000 s^{-1}.

2.3.4 | Membrane casting

Each dope solution was casted onto a glass surface using a doctor blade. The film solution was exposed to air at a baseline evaporation time of 30 s before being immersed in a water nonsolvent bath for 1 minute. For the evaporation time study, the duration of evaporation was expanded to a range of 0, 15, 30, 45, and 60 s. The time it took for each film solution to fully form into a membrane was recorded to investigate the mixing/de-mixing rate. The resulting membranes were immersed in DI water for at least 24 h prior to testing and were stored in DI water. For M3 and M4, the DI water used for membrane storage was replaced each day to remove any residual solvents.

2.4 | Membrane characterization

2.4.1 | Fourier transform infrared spectroscopy

Attenuated total reflection- Fourier transform infrared (ATR-FTIR) (Thermo Nicolet iS50 Fourier transform infrared (FT-IR) spectrometer, Thermo Scientific) was performed to characterize the surface chemical structure of the membranes and to determine the presence of PET in the membrane structure. Each membrane sample was freeze-dried overnight and then placed on the ATR-FTIR crystal (diamond) for analysis.

2.4.2 | Hydrophilicity

The water contact angle of each membrane containing eco-friendly solvents was measured to determine changes in surface hydrophilicity based on the presence of PET. Contact angle was measured using a drop shape analyzer connected to a high-definition camera (DSA 100S, Kruss Companry). One drop containing 12 µl of DI water was deposited on the membrane surface; the interface between the water droplet and membrane surface was captured by the camera and the contact angle was calculated. Ten contact angle measurements were taken, and

TABLE 2 Hansen solubility model calculations for systems containing fabricate polysulfone (PSf), polyethylene terephthalate (PET), PolarClean, and gamma-valerolactone (GVL).

Polymer	δ_d (MPa$^{1/2}$)	δ_p (MPa$^{1/2}$)	δ_h (MPa$^{1/2}$)	R_0
1. PSf	19.7	8.3	8.3	8
2. PET	18.2	6.4	6.6	8

Solvent	δ_d (MPa$^{1/2}$)	δ_p (MPa$^{1/2}$)	δ_h (MPa$^{1/2}$)	R_a	RED
3. PolarClean	15.8	10.7	9.2	1–3: 8.2 2–3: 6.94	1–3: 1.03 2–3: 0.86
4. GVL	19	16.6	7.4	1–4: 8.5 2–4: 10.35	1–4: 1.06 2–4: 1.29
5. PolarClean-GVL	16.6	12.17	8.75	1–5: 7.32 2–5: 6.94	1–5: 0.91 2–5: 0.86

the average values and standard deviations were calculated.

2.4.3 | Scanning electron microscopy imaging

Membrane morphology and surface features were analyzed using scanning electron microscopy (SEM). Sample preparation consisted of immersing and fracturing membrane samples in liquid nitrogen; freeze-dried samples were then coated with colloidal graphite alcohol base and sputter-coated with palladium at a thickness of 3.5 nm. An SEM (Quanta FEG-250 SEM) was used to observe the sample cross-sections.

2.4.4 | Surface pore size analysis

To assess the membrane selectivity, the surface pore size distribution of each membrane was determined using liquid–liquid displacement porometry (LLDP) procedures from a previous study.[33] Membrane samples were dried and wetted with Galwick and IPA before being placed inside a liquid–liquid porometer (LLP-11000A, Porous Materials Incorporated, Ithaca, NY). A pressure range of 0–500 psi was applied within the porometer to drive Galwick to flow through the pores; a scale positioned below the sample measured the mass of the displaced Galwick. The flow pore diameter and bubble point pore diameter distributions were collected.

2.5 | Membrane performance

All filtration experiments were performed in a dead-end filtration cell (Amicon Stirred Cell 50 ml, UFSC05001, provided by Millipore Sigma) at a constant pressure of 4.137 bar (60 psi). To measure the permeability, the membranes were first pre-compacted by filtering DI water for 10 intervals; a bovine serum albumin (BSA) solution of concentration 100 ppm was then filtered through the membrane for 10 intervals. Permeate samples from filtration were analyzed using a UV/Vis spectrophotometer (UV-6300PC, VWR International bvba/sprl, Leuven, Belgium) to measure BSA concentration.[33] All experiments were performed in triplicate to obtain averaged data.

3 | RESULTS AND DISCUSSION

3.1 | Thermodynamic study

3.1.1 | Hansen solubility model

To study the feasibility of PSf and PET interacting with PolarClean and GVL to form a homogenous dope solution, the polymer and solvent affinities were calculated according to the Hansen solubility model. R_a and RED values were calculated for each polymer and solvent (both individually and as a blend) as six pairings: PSf/PolarClean (1–3), PET/PolarClean (2–3), PSf/GVL (1–4), PET/GVL (2–4), PSf/PolarClean-GVL (1–5), PET/PolarClean-GVL (2–5); the parameter, R_a, and RED values for each pair are compiled in Table 2. Hansen solubility parameters of PET, PSf, PolarClean and GVL (δ_d, δ_p, δ_h) used in the calculations were obtained from literature.[28,33]

Solubility parameters for PSf and PET varied with each solvent. The highest RED values for both polymers were associated with GVL, whereas the lowest RED values were associated with the PolarClean-GVL blend. RED values for PSf mixed with PolarClean, GVL, and PolarClean-GVL of 1.03, 1.06, and 0.91 were consistent with the findings of similar studies.[5,33] Since the RED

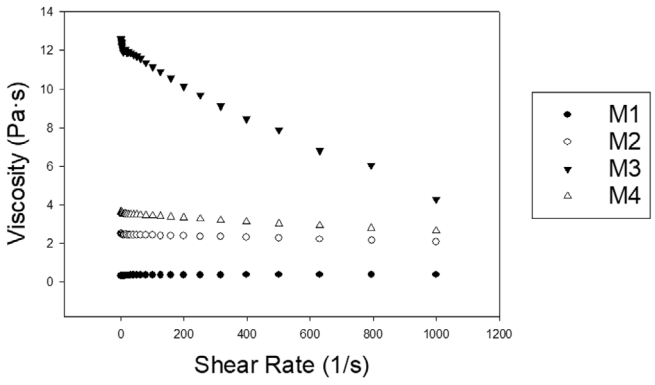

FIGURE 3 Viscosity of each dope solution as a function of shear rate.

values associated with both PSf and PET mixed with PolarClean-GVL were below 1 (0.91 and 0.86, respectively), the Hansen Solubility Model suggested that the solvent blend would have the highest feasibility in dissolving the polymers and form a homogenous dope solution when compared to the individual solvents.

3.2 | Dope solution study results

3.2.1 | PET dissolution study

Despite the Hansen Solubility Model affinity parameters suggesting favorable polymer-solvent affinities, PET and rPET did not completely dissolve in PolarClean and GVL. This empirical result is likely due to the PET composition, as the pristine PET contained glass stabilizers for mechanical strength and the rPET composition was potentially altered due to the manufacturing and recycling processes. Thus, these impurities were not accounted for in the Hansen Solubility Model, appear to inhibit PET dissolution in these solvents, and necessitated the additional solubility study. Each solvent investigated in the solubility study and the respective extent of dissolution is found in Table S1. Partial solubility of PET was observed with several solvents, including ammonium hydroxide, a 50:50 mixture of NaOH-ethylene glycol, and a 50:50 mixture of phenol-DCM. Elevated temperatures above that of room temperature was also required to dissolve PET. Of the potential solvents used, only pure phenol was able to completely dissolve pristine PET. Although phenol presents similar hazards to traditional membrane solvents (e.g., toxicity, irritability), the weight percent used in the dope solutions is significantly lower than the required weight percent of traditional solvents in analogous dope solutions.

3.2.2 | Dope solution viscosity

The dope solution viscosity is a key indicator of the expected dissolution kinetics during NIPS. Low viscosity of the dope solution allows for the solvent and non-solvent to mix and de-mix faster during fabrication, whereas a higher viscosity correlates with slower mixing kinetics. Moreover, the delay in mixing and de-mixing due to a higher viscosity can result in the formation of dense outer membrane layers, which hinders performance.[33]

Viscosities of the dope solutions as a function of shear rate are found in Figure 3. The final viscosity at a shear rate of approximately 1000 s^{-1} was analyzed to estimate the solution viscosity after undergoing the shear forces of doctor blade casting. Of the dope solutions, M1 containing PSf/NMP had the lowest final viscosity of 0.35 Pa s, whereas the presence of green solvents in M2, M3, and M4 resulted in higher final viscosities of 2, 4.3, and 2.6 Pa s, respectively. The trends are consistent with Dong et al.,[33] which also reported an increase in viscosity when PolarClean was present in the dope solution. As such, it was expected that M1 would exhibit faster mixing kinetic during NIPS in comparison to the other solutions. Furthermore, the differences in mixing kinetics were also expected to lead to difference in the membrane morphology.

Over a shear rate range of approximately 1–1000 s^{-1}, each dope solution largely exhibited a linear function with respect to viscosity. In particular, the solution viscosity of M1, M2, and M4 was not significantly altered as shear rate changed, thereby exhibiting Newtonian fluid behavior. Interestingly, the viscosity of M3 differed as shear rate increased by showing relatively greater shear-thinning behavior. The presence of other materials in the "pristine" PET polymer, including glass reinforcers mixed into the pellets, or even special interactions between polymers and solvents during mixing could have potentially contributed to the difference in viscosity and fluid behavior. In general, Newtonian fluid behavior is desired for doctor blade casting since the shear rate is relatively difficult to control manually; as a result, using a solution that can withstand changes in shear rate is more likely to form a desirable membrane.

3.3 | Membrane characterization results

3.3.1 | Fourier transform infrared spectroscopy

FT-IR spectra of M2, M3, and M4 were analyzed to determine the presence of PSf and PET in the latter two membranes. FT-IR spectra of the membranes are found in Figure S1; spectra peaks associated with the primary structures of PSf and PET are found in Tables S2 and S3,

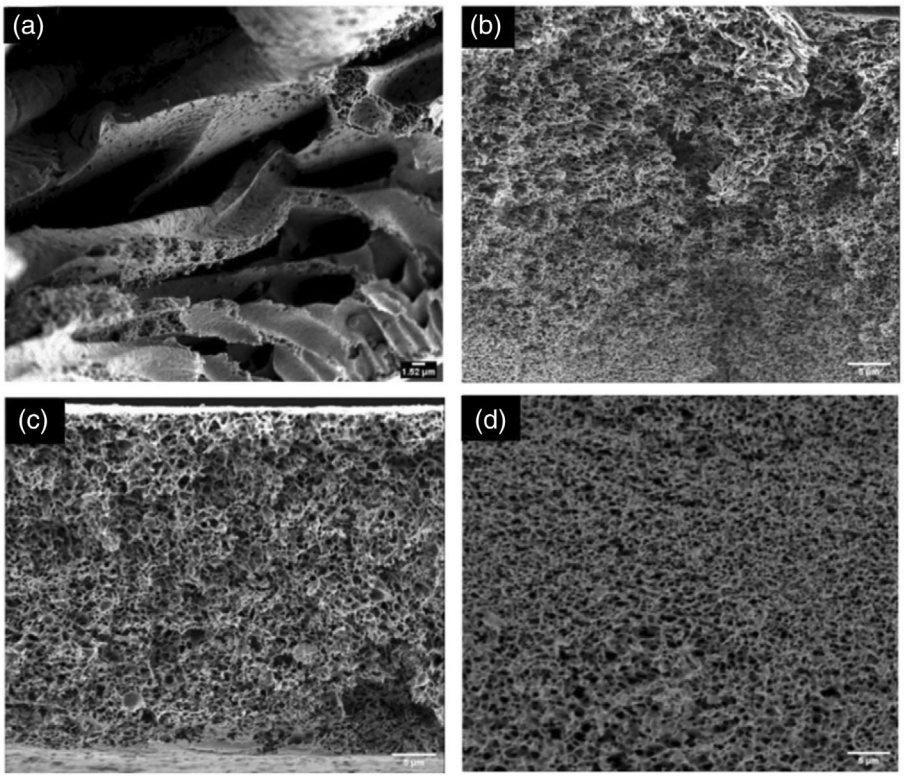

FIGURE 4 Scanning electron microscopy images of the membrane cross-sections for M1 (a), M2 (b), M3 (c), and M4 (d) at an evaporation time of 30 s

respectively.[28,33,38–41] In analysis of the membrane spectra, all three samples exhibited similar spectra profiles, mainly due to the dominant presence of PSf in each membrane. Peaks of all primary structures associated with PSf, including the presence of the C—H (A5), C—SO_2—C (A2, A4), C—O bonds (A3), and the aromatic ring (A1), were observed in each membrane, thus indicating the co-solvents did not affect the membrane chemistry with respect to PSf. The presence of PET in M3 and M4 is evident due to the alteration of the peak at 1651 cm^{-1}, which is distinct in M2 and present as a shoulder in M3 and M4. The appearance of a shoulder in the latter two membranes may indicate the presence of other peaks within the range from 1608–1660 cm^{-1}. Namely, these additional peaks are associated with the C═O in the PET structure, which are also evident in other studies.[28,42] The FT-IR spectra of M3 and M4 also exhibit the characteristic peaks at 1408 cm^{-1} (B1), 1239 cm^{-1} (B2), and 874 cm^{-1} (B3), though these peaks largely overlap with characteristic peaks associated with PSf. Such results were expected due to the relatively minor presence of PET in the dope solution compositions.

3.3.2 | Hydrophilicity

The contact angle measurements between the water droplet and membrane surface for M2, M3, and M4 were measured to evaluate the membrane hydrophilicity and are found in Figure S2. There was a distinct difference in contact angle between membranes that contained PET, as M2 had a contact angle of 99.74 ± 1.09°, whereas M3 and M4 had lower contact angles of 88.36 ± 0.94° and 89.67 ± 1.38°, respectively. High contact angles were expected for each membrane since PSf is hydrophobic.[5] However, the observed decrease in contact angle for M3 and M4 can be attributed to the presence of PET in the membrane, which is hydrophilic due to the high surface energy of the ethylene base.[28] Other studies[28,43,44] have also reported hydrophilicity associated with PET due to the increase in surface energy. Thus, the change in membrane contact angle and hydrophilicity supports the presence of PET present in M3 and M4.

3.3.3 | SEM imaging

Cross sections of each membrane fabricated at the baseline evaporation time are shown in Figure 4. It was observed that the pore structures of the membrane were dependent on the solvents. The use of NMP in M1 (Figure 4a) resulted in the formation of finger-like pore structures, whereas the use of PolarClean and GVL in M2 (Figure 4b), M3 (Figure 4c), and M4 (Figure 4d) led to the formation of finer, sponge-like pore structures. Since the dope solution compositions were relatively similar between M2, M3, and M4, there were no significant

changes found in the cross-section structures. Furthermore, the differences in pores structure correlate with the differences in the dope solution viscosities. Dope solutions with a low viscosity (M1) tend to exhibit faster mixing and de-mixing phenomena during phase inversion, whereas this process is decelerated with dope solutions with higher viscosity (M2, M3, and M4). As such, the cross-sectional morphology of the membranes was consistent with the trends in dope solution viscosity. Moreover, it was expected that the membrane performance trends would also differ due to the morphological differences since other studies have reported higher water flux with membranes having finger-like pore structures.[5,33]

3.3.4 | Surface pore size analysis

Similar to the membrane morphology, the surface pore size distribution differed with the dope solution composition. Triplicate measurements of the pore diameter and the bubble point pore diameter distributions (i.e., the largest pore size on the membrane surface) for each membrane are listed in Table 3. The membranes M1, M3, and M4 were found to have pore sizes within the lower spectrum of the UF mean pore size range, which was consistent with lower permeability that was observed. In contrast, M2 exhibited the highest permeability, thus correlating with the nearly 10-fold increase in pore size.

TABLE 3 Membrane surface pore measurements.

Membrane	Pore diameter (μm)	Bubble point pore diameter (μm)
M1	0.0047 ± 0.001	0.005 ± 0.0002
M2	0.0414 ± 0.008	0.064 ± 0.006
M3	0.0040 ± 0.0002	0.022 ± 0.005
M4	0.0076 ± 0.0005	0.032 ± 0.001

Despite also having PolarClean and GVL as solvents, the presence of PET-phenol in M3 and M4 likely contributed to the decrease in pore size.

The pore size distributions for each membrane are found in Figure S3. Based on the pore size distributions, several membranes exhibited a nonuniform mean pore distribution, most notably in the pore size distributions of M2. These distributions indicate the presence of larger pores or microvoids within the structure, which is also supported by the larger differences between mean pore size and the bubble point pore diameter for M2, M3, and M4. The larger variations in the pore size could influence the membrane performance by creating spaces for particles to pass through more easily.

3.4 | Membrane filtration results

As previously noted, differences in the dope solution viscosities and resulting membrane morphologies would suggest differences in the membrane performance. Membrane permeability of pure DI water during membrane pre-compaction and of the BSA solution during filtration is found in Figure 5a. By the conclusion of pre-compaction, the permeability stabilized for each membrane with final pre-compaction permeabilities of 154.5 LMH/bar, 201.9, 54.5, and 36.1 LMH/bar for M1, M2, M3, and M4, respectively. The order of permeability was largely consistent following BSA filtration with final values of 22.6, 36.5, 18.6, and 23.4 LMH/bar for M1, M2, M3, and M4, respectively.

Consistent general trends were observed for each membrane, including the decrease in permeability as filtration progressed likely due to BSA fouling on the membrane surface. Stability in the filtration permeability differed for each type. The addition of the PET-phenol M3 and M4 resulted in a significant decrease in permeability as compared to M2. Of the two PET membranes, however,

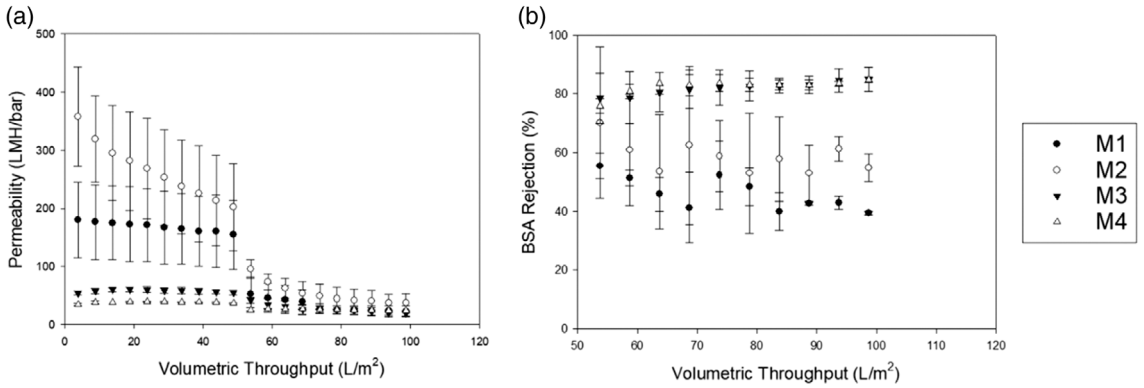

FIGURE 5 Permeability (a) and bovine serum albumin (BSA) rejection (b) of each membrane at a baseline evaporation time of 30 s

M4 exhibited a more stable permeability profile throughout filtration with reduced effects of particle fouling. The lower permeabilities of M3 and M4 correlate with the smaller mean pore sizes that were measured, indicating a direct relationship between permeability and mean pore size. Indeed, the mean pore size of M2 was the largest of all membranes, which also exhibited the highest permeability during pre-compaction and filtration.

BSA rejection during filtration for each membrane is found in Figure 5b. Similar profiles to those found in permeability were evident in BSA rejection. M1 exhibited the lowest maximum rejection capability of 55.4% that ultimately decreased over the course of filtration. As found in Dong et al.,[33] M2 exhibited an increased maximum rejection capability of 70.1% before decreasing during filtration. M3 and M4 showed similar rejection profiles that were more stable as a function of volumetric throughput; maximum rejections of approximately 84.9% were observed for both PET membranes. The similarity in rejection profiles of the two membranes was expected due to the similarity in dope solution composition, though the presence of the PET may have contributed to the improvement in BSA rejection in comparison to M1 and M2.

Overall, rejection largely remained stable over the course of filtration, though minor fluctuations were observed in the profiles of M1 and M2. Increases in rejection as a function of volumetric throughput, as noted in each membrane, is likely the result of BSA fouling on the membrane surface. In the case of M1 and M2, observed decreases in the rejection may be attributable to instability of the membrane structure, thus compromising the selectivity; however, the minor extent of instability and the coupled effects of BSA fouling appear to have curtailed significant declines in BSA rejection.

3.5 | Evaporation time study results

3.5.1 | Phase separation study

During membrane casting, the time it took for the casted film solutions to fully undergo phase inversion and form membranes was recorded to investigate the relationship between evaporation time and the rate of mixing/de-mixing in the system. The time before membrane formation for each dope solution is found in Figure 6. Across all solutions, there was a direct relationship observed for the time before formation and evaporation time; that is, the time for each membrane to fully form increased as evaporation time increased. As such, the rate of mixing/de-mixing decreased with increasing evaporation time, which confirms the thickening of the "skin" layer at the top of the membrane that has been observed in other evaporation time studies.[5,45,46] As more solvent evaporates into the air during the evaporation step, the "skin" layer becomes denser with a polymer-heavy concentration and acts a resistance barrier during NIPS.[10]

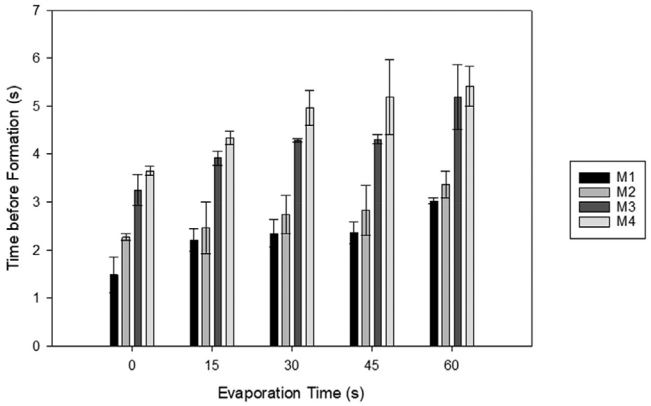

FIGURE 6 Time before membrane formation for each solution.

3.5.2 | Membrane morphology

Along with the baseline evaporation time of 30 s, additional intervals of 0, 15, 45, and 60 s were used in the membrane fabrication process. SEM images of the cross-sectional areas of each membrane at evaporation times of 0, 30, and 60 s are shown in Figure 7 and illustrate differences in the cross-sectional morphology with respect to dope solution composition and evaporation time. The cross-sections of M1 exhibited finger-like pore structures that were consistent with the findings from literature. The shape of the pores was also indicative of lower dope solution viscosity and the subsequent faster mixing and de-mixing during phase inversion. As evaporation time increased, however, the cross-sections exhibited more sponge-like pores alongside the finger-like pore structures, indicating that the mixing and de-mixing process deaccelerated.

The sponge-like pore structures comprised the morphology of M2, M3, and M4, which was consistent with the higher viscosities of the respective dope solutions. Overall, evaporation time did not result in significant alterations in the cross-sectional morphology of the membranes. Instead, it is suggested that any alterations in the membrane morphology were largely localized to the skin layer at top surface. As evaporation time increased, the increased solvent evaporation from the top layer would have led to a thicker skin layer. As such, differences in the membrane performance with respect to evaporation time were expected due to the resulting delays in diffusion during NIPS and permeability during filtration at the skin layer.

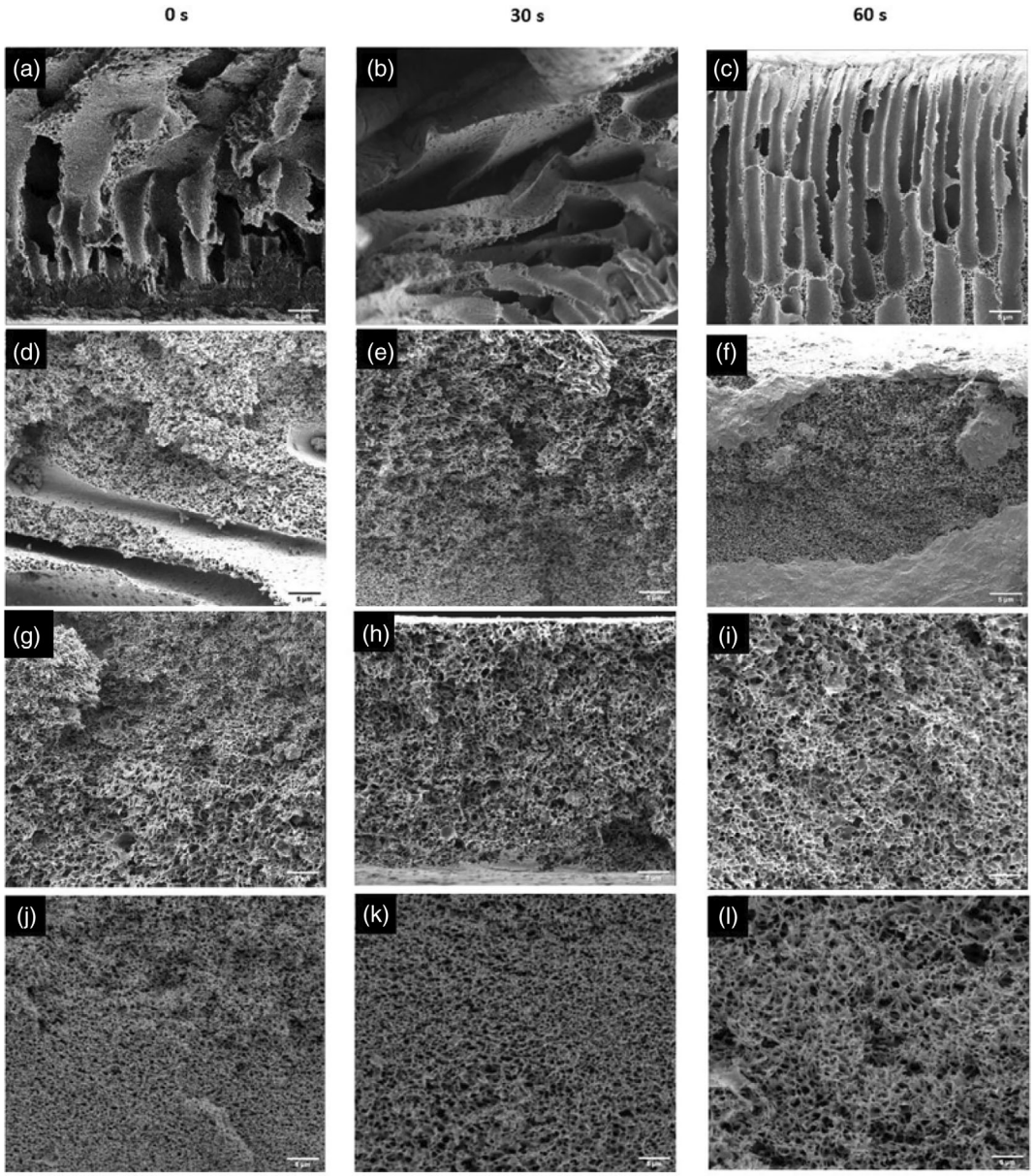

FIGURE 7 Scanning electron microscopy images of the cross-sections of M1 (a–c), M2 (d–f), M3 (g–i), and M4 (j–l) at evaporation time intervals of 0, 30, and 60 s; magnification of 2500×

3.5.3 | Membrane performance

With probable changes in the skin layer thickness, changes in the membrane performance were expected. Permeability of each membrane at different evaporation times is found in Figure 8. Overall, general trends found in membrane permeability were consistent with literature in that increasing the evaporation time resulted in decreased permeability. By increasing the evaporation time to 60 s, M1, M2, M3, and M4 exhibited a 33.9, 48.4, 1.8, and 32.4 LMH/bar average decrease in permeability at the end of pre-compaction, respectively. In contrast, decreasing the evaporation time to 0 s resulted in M1, M2, M3, and M4 exhibiting a 139.4, 55.7, 846.1, and 235.8 LMH/bar average increase in permeability at the end of pre-compaction, respectively. These trends were also generally evident when the evaporation time was changed to 15 and 45 s, though several irregular changes were also observed, such as the increase in permeability for M1 at 45 s and for M2 at 15 s. These minor inconsistencies could be attributed to the condition of the membranes, as several human and environmental factors during the blade casting process can lead to minor alterations between each membrane sheet that affect performance. Nevertheless, the cross-section morphologies and general trends in permeability indicate that the thickness of the skin layer is dependent on evaporation time, though the extent of layer thickening may depend on the membrane materials.

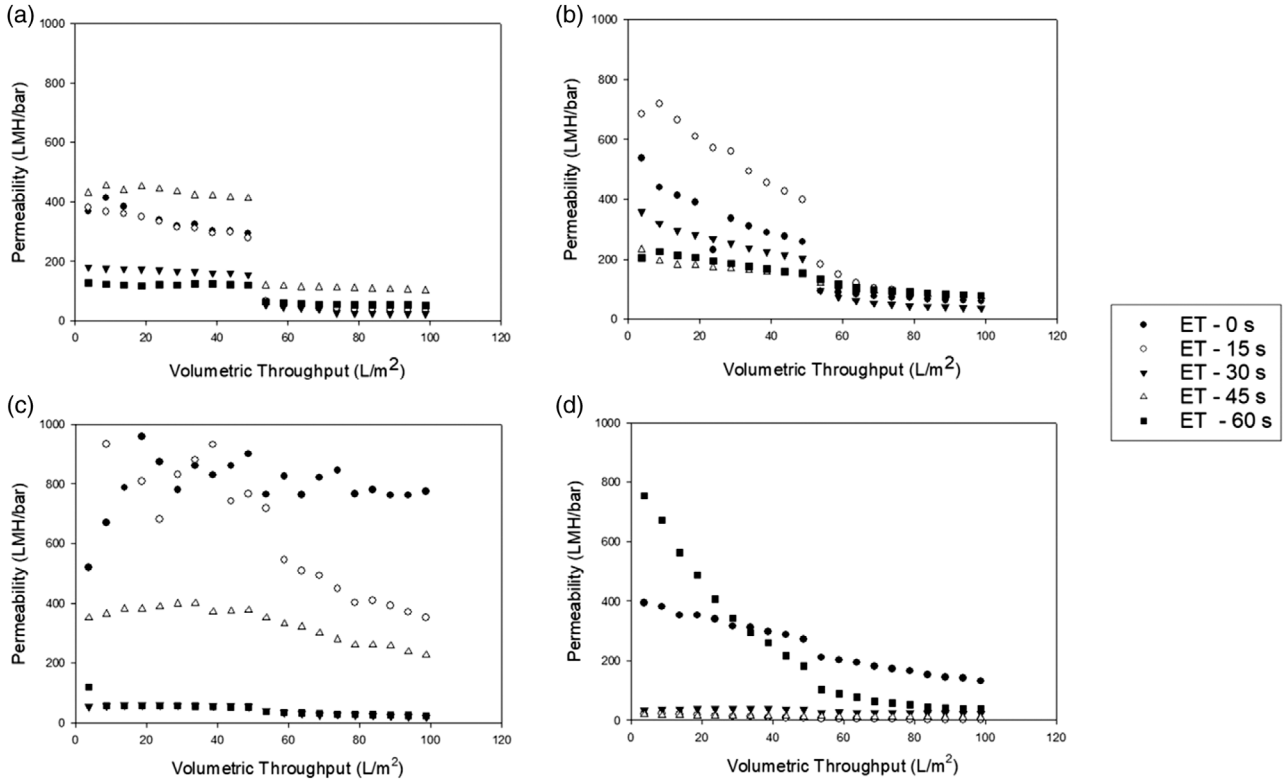

FIGURE 8 Permeability of M1 (a), M2 (b), M3 (c), and M4 (d) membranes with respect to evaporation time

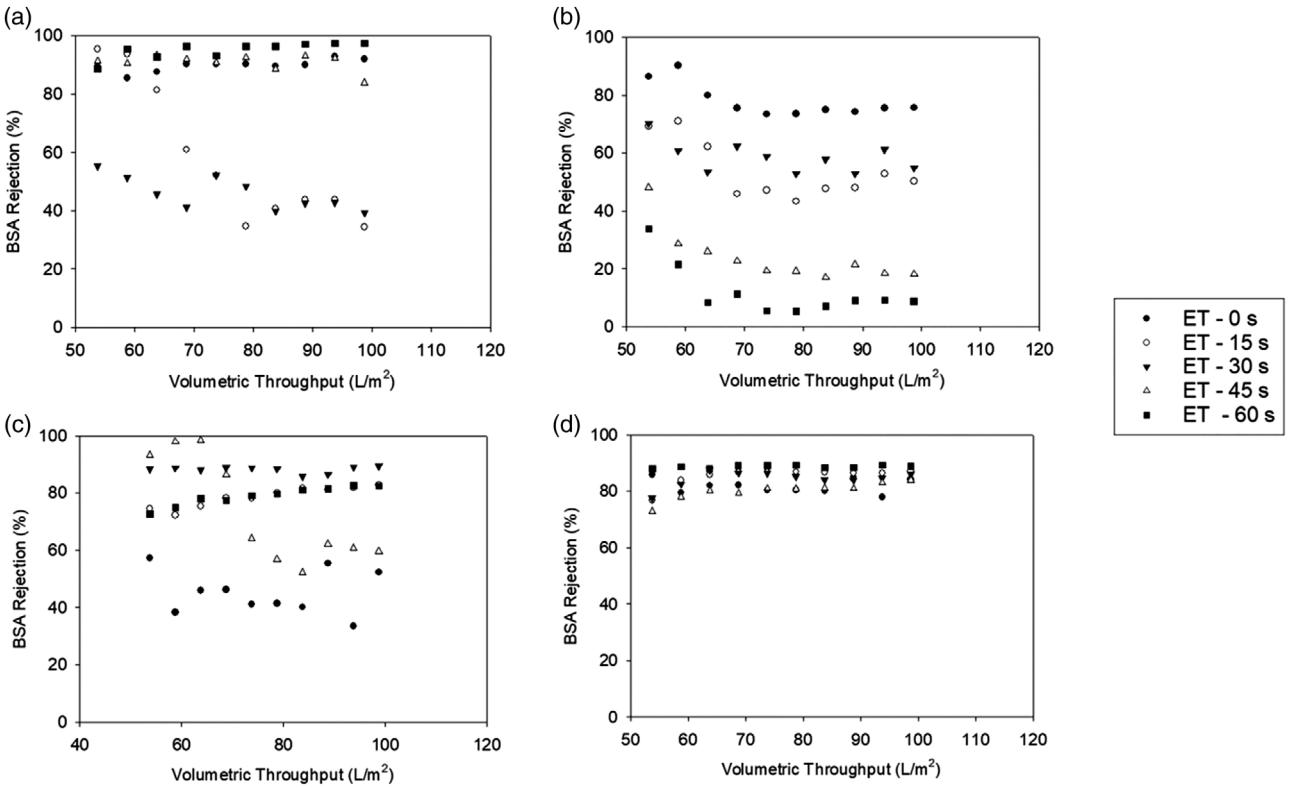

FIGURE 9 Bovine serum albumin (BSA) rejection of M1 (a), M2 (b), M3 (c), and M4 (d) membranes with respect to evaporation time

In further analysis of the permeability trends, optimizing green material-based membrane performance with respect to evaporation time can also be posited. At higher evaporation times (i.e., 30, 45, and 60 s), M2 largely exhibited higher permeability compared to M1, though the addition of PET in M3 and M4 led to significant decreases in permeability. However, such significant alterations were not evident at lower evaporation times (i.e., 0 s, 15), as M3 and M4 retained relatively high average permeabilities of 773.5 LMH/bar and 131.8 LMH/bar, respectively, at the conclusion of BSA filtration. As such, a UF membrane that incorporates recycled PET and PolarClean-GVL can attain or even exceed the permeability profile of a traditional UF membrane (M1) by decreasing the evaporation time from the baseline conditions during fabrication. In short, evaporation time can be used as a tool to "equalize" membrane performance across different membrane compositions, thereby avoiding the drawback of lower permeability found at baseline conditions.

The relationship between evaporation time and BSA rejection was also assessed for each membrane. Figure 9 illustrates the BSA rejection profiles of each membrane at different evaporation times. Compared to the results at the baseline evaporation time, BSA rejection varied with respect to volumetric throughput. In several cases, BSA rejection profiles at lower evaporation times (i.e., 0 s, 15 w, 30 s) were generally more variable, whereas the profiles at higher evaporation times (i.e., 45 s, 60 s) exhibited relatively more stability. M1 BSA rejection underwent a 28.9% decline during filtration at the baseline evaporation time compared to a 9.1% increase at an evaporation time of 60 s; similarly, M4 BSA rejection experienced a 9.8% increase at the baseline evaporation time compared to a 1.1% increase at an evaporation time of 60 s. In other cases, instability was found in BSA rejection profiles even at higher evaporation times, such as a 11.9% increase in BSA M3 BSA rejection at an evaporation time of 60 s compared to a 1.2% increase in rejection at the baseline evaporation. As stated earlier, such variations were likely due to the occurrence of fouling or a compromise in membrane stability.

Contrary to the noted trends in permeability, BSA rejection largely followed a reciprocal pattern. Namely, BSA rejection improved as evaporation time increased, as seen in M1, M3, and M4. By increasing the evaporation time from 0 to 60 s, the final M1 BSA rejection increased from 91.9% to 97.4%, M3 BSA rejection increased from 52.3% to 82.5%, and M4 BSA rejection increased from 84.1% to 88.9%. Again, minimal changes in the membrane cross-section over evaporation time suggest that the increase in rejection is attributable to other factors. The likely thickening of the membrane skin layer plays a probable role by slowing the water flux and permeability, thereby reducing the stresses on the membrane that could compromise the stability and selectivity. However, M2 exhibited a rejection profile with opposite trends of the other membranes with decreasing BSA rejection as evaporation time increased. In fact, the final M2 BSA rejection decreased from 75.6% to 8.7% (by increasing the evaporation time from 0 to 60 s). While unexpected, differences in rejection profile were likely due to the inclusion or exclusion of specific materials in each dope solution. In this case, the M2 dope solution composition may uniquely lead to such an opposite trend. As noted by Holda et al.,[10] contradicting findings on the effect of evaporation time on membrane rejection capabilities have been found, which suggests that the influence may be uniquely dependent on membrane composition.

Despite the potential unique effect of evaporation time, optimization of membrane rejection capabilities can still be posited using this fabrication condition. In examination of the rejection profiles of each membrane, similarities in trends can be identified that can be used to "equalize" membrane performance across different membrane compositions. Focusing on the incorporation of green materials, M4 exhibited a stable BSA rejection profile between 87.9% and 89.2% at an evaporation time of 60 s, placing it above the BSA rejection profile of M1 at the baseline evaporation time and 8.2% lower than the maximum BSA rejection of M1 at an evaporation time of 60 s. In summary, increasing the evaporation time of recycled PET-based membranes may result in stable rejection profiles that are comparable to those using traditional materials. However, this conclusion presents a general tradeoff between permeability and rejection with respect to evaporation time. Fabrication of M4 at the baseline evaporation time would lead to a compromise of modest permeability and rejection capabilities, though less competitive with the performance profile of M1.

4 | CONCLUSION

In light of new regulations on traditional membrane solvents, the need for utilizing eco-friendly alternatives has become more imperative. In this study, PSf Uf membranes were fabricated using a PolarClean-GVL solvent mixture and rPET as materials with more eco-friendly properties than traditional membrane materials. The Hansen Solubility Model calculations of the system indicated favorable dissolution of the materials and formation of a membrane via NIPS. When fabricated at an evaporation time of 30 s, the PET-PSf/PolarClean-GVL membranes filtered BSA at a 3.5% higher permeability (23.4 LMH/bar) and 53.2% greater rejection (84.9%) than

traditional PSf/NMP membranes. Increasing the evaporation time to 60 s resulted in a decrease in permeability and increase in BSA rejection (32.4 LMH/bar decrease in permeability and 0.8% increase in BSA rejection for M4); decreasing the evaporation time to 0 generally led to the opposite trends (235.8 LMH/bar increase in permeability and 4% increase in BSA rejection for M4). Dope solution viscosity, pore structure morphology, and pore size distributions correlated with the performance differences between membrane types. It is important to note that a novel combination of eco-friendly materials was effectively utilized in fabricating a polymeric membrane rather than the fabrication of an entirely eco-friendly polymeric membrane. Since the use of phenol as an intermediate solvent limits the eco-friendly properties of the membranes, identifying an eco-friendly solvent capable of complete PET dissolution would remove a significant barrier in utilizing the material as an eco-friendly polymer. Coupled with capitalizing on the value of adjusting evaporation time during fabrication, eco-friendly UF membranes with optimized performance capabilities appear to be a promising solution to a currently unsustainable separations field.

AUTHOR CONTRIBUTIONS

Alex Williams: Data curation (supporting); investigation (supporting). **David Lu:** Data curation (equal); formal analysis (equal); investigation (equal); writing – original draft (equal). **Isabel C. Escobar:** Conceptualization (lead); funding acquisition (lead); project administration (lead); writing – review and editing (lead). **Kassandra Opfar:** Data curation (supporting); formal analysis (supporting). **Parker Nurick:** Data curation (supporting); formal analysis (supporting). **Parto Babaniamansour:** Formal analysis (equal); investigation (equal); writing – original draft (equal).

ACKNOWLEDGMENTS

The authors want to acknowledge that this work was supported by the National Science Foundation (grant numbers 2121674 and 1922694). The authors also want to acknowledge Solvay Novecare for providing PolarClean, and all imaging was possible thanks to Kentucky IDeA Networks of Biomedical Research Excellence (KY-INBRE) grant P20GM103436. The graphical abstract was created with Biorender.com.

DATA AVAILABILITY STATEMENT

The data that support the findings of this study are available from the corresponding author upon reasonable request.

ORCID

Isabel C. Escobar https://orcid.org/0000-0001-9269-5927

REFERENCES

[1] T. Peters, *Chem. Eng. Technol.* **2010**, *33*, 1233.
[2] S. Acarer, İ. Pir, M. Tüfekci, G. Türkoğlu Demirkol, N. Tüfekci, *Polymer* **2021**, *13*, 1661.
[3] D. M. Warsinger, S. Chakraborty, E. W. Tow, M. H. Plumlee, C. Bellona, S. Loutatidou, L. Karimi, A. M. Mikelonis, A. Achilli, A. Ghassemi, L. P. Padhye, S. A. Snyder, S. Curcio, C. D. Vecitis, H. A. Arafat, J. H. Lienhard, *Prog. Polym. Sci.* **2018**, *81*, 209.
[4] C. Kahrs, J. Schwellenbach, *Polymer* **2020**, *186*, 122071.
[5] X. Dong, A. Al-Jumaily, I. C. Escobar, *Membranes* **2018**, *8*, 23.
[6] B. McVerry, M. Anderson, N. He, H. Kweon, C. Ji, S. Xue, E. Rao, C. Lee, C.-W. Lin, D. Chen, D. Jun, G. Sant, R. B. Kaner, *Nano Lett.* **2019**, *19*, 5036.
[7] H. Kweon, C.-W. Lin, M. M. Faruque Hasan, R. Kaner, G. N. Sant, *ACS Appl. Polym. Mater.* **2019**, *1*, 3233.
[8] B. S. Lalia, V. Kochkodan, R. Hashaikeh, N. Hilal, *Desalination* **2013**, *326*, 77.
[9] A. S. Wittmar, D. Koch, O. Prymak, M. Ulbricht, *ACS Omega* **2020**, *5*, 27314.
[10] A. K. Hołda, I. F. Vankelecom, *J. Appl. Polym. Sci.* **2015**, *132*, 42130.
[11] J. U. Garcia, T. Iwama, E. Y. Chan, D. R. Tree, K. T. Delaney, G. H. Fredrickson, *ACS Macro Lett.* **2020**, *9*, 1617.
[12] X. Dong, D. Lu, T. A. L. Harris, I. C. Escobar, *Membranes* **2021**, *11*, 309.
[13] Q. Wu, W. Xie, H. Wu, L. Wang, S. Liang, H. Chang, B. Liu, *RSC Adv.* **2019**, *9*, 34486.
[14] J. H. Clark, S. J. Tavener, *Org. Process. Res. Dev.* **2007**, *11*, 149.
[15] P. G. Jessop, *Green Chem.* **2011**, *13*, 1391.
[16] C. Capello, U. Fischer, K. Hungerbühler, *Green Chem.* **2007**, *9*, 927.
[17] M. Razali, J. F. Kim, M. Attfield, P. M. Budd, E. Drioli, Y. M. Lee, G. Szekely, *Green Chem.* **2015**, *17*, 5196.
[18] G. R. Guillen, Y. Pan, M. Li, E. M. Hoek, *Ind. Eng. Chem. Res.* **2011**, *50*, 3798.
[19] B. van der Bruggen, *J. Appl. Polym. Sci.* **2009**, *114*, 630.
[20] F. Liu, N. A. Hashim, Y. Liu, M. R. M. Abed, K. Li, *J. Membr. Sci.* **2011**, *375*, 1.
[21] F. Galiano, K. Briceño, T. Marino, A. Molino, K. V. Christensen, A. Figoli, *J. Membr. Sci.* **2018**, *564*, 562.
[22] Y. Medina-Gonzalez, P. Aimar, J.-F. Lahitte, J.-C. Remigy, *Int. J. Sustainable Eng.* **2011**, *4*, 75.
[23] T. Marino, E. Blasi, S. Tornaghi, E. Di Nicolò, A. Figoli, *J. Membr. Sci.* **2018**, *549*, 192.
[24] R. Jacquot and P. Marion, Process for producing compounds comprising nitrile functions. Google Patents. **2015**
[25] B. Girisuta, L. Janssen, H. Heeres, *Green Chem.* **2006**, *8*, 701.
[26] F. Alvarado Chacon, M. T. Brouwer, E. U. T. van Velzen, *Packag. Technol. Sci.* **2020**, *33*, 347.
[27] I. Taniguchi, S. Yoshida, K. Hiraga, K. Miyamoto, Y. Kimura, K. Oda, *ACS Catal.* **2019**, *9*, 4089.
[28] B. A. Pulido, O. S. Habboub, S. L. Aristizabal, G. Szekely, S. P. Nunes, *ACS Appl. Polym. Mater.* **2019**, *1*, 2379.
[29] H. N. Doan, P. P. Vo, K. Hayashi, K. Kinashi, W. Sakai, N. Tsutsumi, *J. Environ. Chem. Eng.* **2020**, *8*, 103921.
[30] N. Arahman, A. Fahrina, S. Amalia, R. Sunarya, S. Mulyati, *F1000Research* **2017**, *6*, 668.

[31] N. T. Hassankiadeh, Z. Cui, J. H. Kim, D. W. Shin, S. Y. Lee, A. Sanguineti, V. Arcella, Y. M. Lee, E. Drioli, *J. Membr. Sci.* **2015**, *479*, 204.
[32] J. T. Jung, J. F. Kim, H. H. Wang, E. Di Nicolo, E. Drioli, Y. M. Lee, *J. Membr. Sci.* **2016**, *514*, 250.
[33] X. Dong, H. D. Shannon, C. Parker, S. De Jesus, I. C. Escobar, *AIChE J* **2020**, *66*, e16790.
[34] C. M. Hansen, *Hansen Solubility Parameters: A User's Handbook*, CRC Press, Boca Raton, FL **2007**.
[35] X. Dong, T. J. Jeong, E. Kline, L. Banks, E. Grulke, T. Harris, I. C. Escobar, *J. Membr. Sci.* **2020**, *614*, 118510.
[36] P. P. Vo, H. N. Doan, K. Kinashi, W. Sakai, N. Tsutsumi, D. P. Huynh, *Polymer* **2018**, *10*, 680.
[37] I. Strain, Q. Wu, A. M. Pourrahimi, M. S. Hedenqvist, R. T. Olsson, R. L. Andersson, *J. Mater. Chem. A* **2015**, *3*, 1632.
[38] M. Saxena, S. Sharma, A. Bhattacharya, *J. Membr. Sci. Technol.* **2015**, *2*, 39.
[39] A. Mushtaq, H. B. Mukhtar, A. M. Shariff, *Res. J. Appl. Sci. Eng. Technol.* **2014**, *7*, 1811.
[40] S. Vico, B. Palys, C. Buess-Herman, *Langmuir* **2003**, *19*, 3282.
[41] M. Peltzer, C. Simoneau, *Report of an Interlaboratory Comparison from the European Reference Laboratory for Food Contact: ILC002 2013—Identification of Polymeric Materials*, Publications Office of the European Union, Luxembourg **2013**.
[42] C. Ioakeimidis, K. N. Fotopoulou, H. K. Karapanagioti, M. Geraga, C. Zeri, E. Papathanassiou, F. Galgani, G. Papatheodorou, *Sci. Rep.* **2016**, *6*, 23501.
[43] S. Jasmee, G. Omar, N. Masripan, A. A. Kamarolzaman, A. Ashikin, F. C. Ani, *Mater. Res. Exp.* **2018**, *5*, 96304.
[44] D. Jucius, V. Grigaliūnas, V. Kopustinskas, A. Lazauskas, A. Guobienė, *Appl. Surf. Sci.* **2012**, *263*, 722.
[45] A. K. Hołda, B. Aernouts, W. Saeys, I. F. J. Vankelecom, *J. Membr. Sci.* **2013**, *442*, 196.
[46] P. Vandezande, X. Li, L. E. Gevers, I. F. Vankelecom, *J. Membr. Sci.* **2009**, *330*, 307.

SUPPORTING INFORMATION

Additional supporting information can be found online in the Supporting Information section at the end of this article.

How to cite this article: D. Lu, P. Babaniamansour, A. Williams, K. Opfar, P. Nurick, I. C. Escobar, *J. Appl. Polym. Sci.* **2022**, e52823. https://doi.org/10.1002/app.52823